

perovskite-type compounds $[(1-x)\text{La}, x\text{Ca}]\text{MnO}_3$. *Phys. Rev.* **100**, 545–563 (1955).

19. Matsumoto, G. Study of $(\text{La}_{1-x}\text{Ca}_x)\text{MnO}_3$. I. Magnetic structure of LaMnO_3 . *J. Phys. Soc. Jpn* **29**, 606–615 (1970).

20. Kaplan, M. D. & Vekhter, B. G. *Cooperative Phenomena in Jahn-Teller Crystals* (Plenum, New York, 1995).

21. Saitoh, T. *et al.* Electronic structure of $\text{La}_{1-x}\text{Sr}_x\text{MnO}_3$ studied by photoemission and x-ray absorption spectroscopy. *Phys. Rev. B* **51**, 13942–13951 (1995).

22. Arima, T. & Tokura, Y. Optical study of electronic structure in perovskite-type RMO_3 ($R = \text{LaY}; M = \text{Sc, Ti, V, Cr, Mn, Fe, Co, Ni, Cu}$). *J. Phys. Soc. Jpn* **64**, 2488–2501 (1995).

23. Iliiev, M. N. *et al.* Raman spectroscopy of orthorhombic perovskite YMnO_3 and LaMnO_3 . *Phys. Rev. B* **57**, 2872–2877 (1998).

24. Yamamoto, K., Kimura, T., Ishikawa, T., Katsufuji, T. & Tokura, Y. Raman spectroscopy of the charge-orbital ordering in layered manganites. *Phys. Rev. B* **61**, 14706–14715 (2000).

25. Podobedov, V. B., Weber, A., Romero, D. B., Rice, J. P. & Drew, H. D. Effect of structural and magnetic transitions in $\text{La}_{1-x}\text{M}_x\text{MnO}_3$ ($M = \text{Sr, Ca}$) single crystals in Raman scattering. *Phys. Rev. B* **58**, 43–46 (1998).

26. Abrashev, M. V. *et al.* Comparative study of optical phonons in the rhombohedrally distorted perovskites LaAlO_3 and LaMnO_3 . *Phys. Rev. B* **59**, 4146–4153 (1999).

27. Inoue, J. *et al.* Raman scattering by orbital waves in perovskite LaMnO_3 . *Physica B* **237–238**, 51–53 (1997).

28. Schaack, G. in *Light Scattering in Solids VII* (eds Cardona, M. & Güntherodt, G.) 24–173 (Springer, Berlin, 2000).

29. Mitchell, J. F. *et al.* Structural phase diagram of $\text{La}_{1-x}\text{Sr}_x\text{MnO}_{3+\delta}$: Relationship to magnetic and transport properties. *Phys. Rev. B* **54**, 6172–6183 (1996).

30. Hirota, K., Kaneko, N., Nishizawa, A. & Endoh, Y. Two-dimensional planar ferromagnetic coupling in LaMnO_3 . *J. Phys. Soc. Jpn* **65**, 3736–3739 (1996).

Acknowledgements

We thank N. Nagaosa, T. Katsufuji, P. Prelovšek and S. E. Barnes for discussions. This work was supported in part by NEDO Japan, CREST Japan, the Science and Technology Special Coordination Fund for Promoting Science and Technology, and Grant-in-Aid for Scientific Research Priority Area from the Ministry of Education, Science and Culture of Japan. S.O. acknowledges the financial support of JSPS. Part of the numerical calculation was performed in the supercomputing facilities in IMR, Tohoku University.

Correspondence and requests for materials should be addressed to Y.T. (e-mail: tokura@ap.t.u-tokyo.ac.jp).

Coherent branched flow in a two-dimensional electron gas

M. A. Topinka*, B. J. LeRoy†, R. M. Westervelt*‡, S. E. J. Shaw†, R. Fleischmann‡, E. J. Heller†§, K. D. Maranowski|| & A. C. Gossard||

* Division of Engineering and Applied Sciences, † Department of Physics, § Department of Chemistry and Chemical Biology, Harvard University, Cambridge, Massachusetts 02138, USA
 ‡ Max-Planck-Institut für Strömungsforschung, Bunsenstrasse 10, D-37073 Göttingen, Germany
 || Materials Department, University of California, Santa Barbara, California 93106, USA

Semiconductor nanostructures based on two-dimensional electron gases (2DEGs) could form the basis of future devices for sensing, information processing and quantum computation. Although electron transport in 2DEG nanostructures has been well studied, and many remarkable phenomena have already been discovered (for example, weak localization, quantum chaos, universal conductance fluctuations^{1,2}), fundamental aspects of the electron flow through these structures have so far not been clarified. However, it has recently become possible to image current directly through 2DEG devices using scanning probe microscope techniques^{3–13}. Here, we use such a technique to observe electron flow through a narrow constriction in a 2DEG—a quantum point contact. The images show that the electron flow from the point contact forms narrow, branching strands instead of smoothly spreading fans. Our theoretical study of this flow indicates that this branching of current flux is due to focusing of the electron paths by ripples in the background potential. The strands are decorated by interference fringes separated by half the Fermi wavelength, indicating the persistence

of quantum mechanical phase coherence in the electron flow. These findings may have important implications for a better understanding of electron transport in 2DEGs and for the design of future nanostructure devices.

Images of electron flow from the quantum point contact (QPC) are obtained by raster scanning a negatively charged scanning probe microscope (SPM) tip above the surface of the device and simultaneously measuring the position-dependent conductance of the device. The negatively charged tip capacitively couples to the 2DEG, creating a depletion region that backscatters electron waves. When the tip is positioned over areas with high electron flow from the QPC, the conductance is decreased, whereas when the tip is over areas of relatively low electron flow the conductance is unmodified. By raster scanning the tip over the sample, a two-dimensional image of electron flow can be obtained.

The QPC sample is mounted in an atomic force microscope and cooled to liquid He temperatures. The QPC is formed in the 2DEG inside a GaAs/AlGaAs heterostructure by negatively biasing two gates on the surface—a negative potential on these gates creates two depletion regions that define a variable-width channel between them, as shown in Fig. 1a. The heterostructure for the devices used in this experiment was grown by molecular beam epitaxy on an n-type GaAs substrate. The 2DEG resides 57 nm below the surface with mobility $\mu = 1.0 \times 10^6 \text{ cm}^2 \text{ V}^{-1} \text{ s}^{-1}$ and density $n = 4.5 \times 10^{11} \text{ cm}^{-2}$. These values of mobility and density correspond to a mean free path $l = 11 \mu\text{m}$, Fermi wavelength $\lambda_F = 37 \text{ nm}$, and

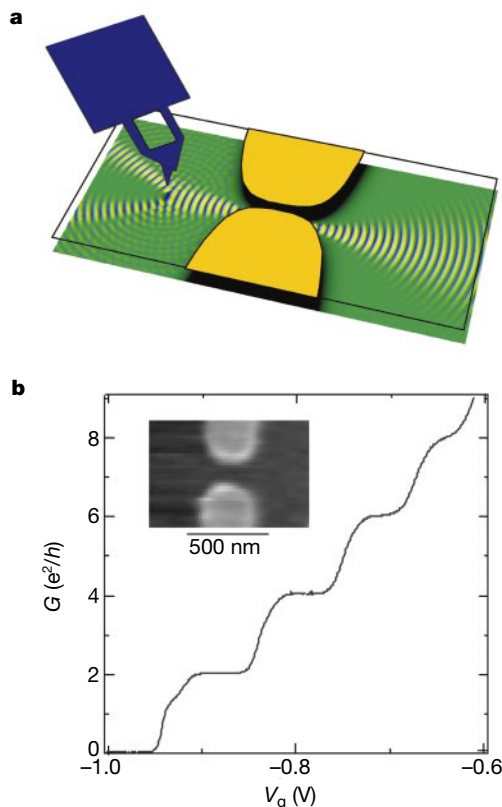


Figure 1 Experimental set-up. **a**, Schematic diagram of the experimental set-up used for imaging electron flow. The tip introduces a movable depletion region which scatters electron waves flowing from the quantum point contact (QPC). An image of electron flow is obtained by measuring the effect the tip has on QPC conductance as a function of tip position. Two ohmic contacts $\sim 1 \mu\text{m}$ away from the QPC (not shown) allow the conductance of the QPC to be measured using an a.c. lock-in amplifier at 11 kHz. The root-mean-square voltage across the QPC, 0.2 mV, was chosen in order not to heat electrons significantly above the lattice temperature of 1.7 K. **b**, Conductance of the QPC used for Fig. 2b versus QPC width controlled by the gate voltage. Steps at integer multiples of $2e^2/h$ are clearly visible. The inset is a topographic AFM image of the QPC.

Fermi energy $E_F = 16$ meV. The conductance of the QPC, shown in Fig. 1b, increases as the width of the channel is increased (by changing the gate voltage V_g) and shows well defined conductance plateaus at integer multiples of the conductance quantum $2e^2/h$ (refs 1, 2).

Figure 2a and b shows images of electron flow from two different QPCs at the temperature 1.7 K; both QPCs are biased on the $G = 2e^2/h$ conductance plateau. Figure 2b shows the flow patterns on each side of a QPC and Fig. 2a shows a higher-resolution image of flow from one side of a different QPC. In both these images, the current leaves the point contact in a central lobe, as expected from an exact quantum-mechanical calculation of electron flow through an ideal QPC. Rather than continuing out as a smoothly widening fan, it quickly forks into several different paths and continues to branch off into ever smaller rivulets for the full width of the scan. This branching behaviour was observed in all of the 13 QPC exit patterns observed so far. Previously, there have been suggestions of an unexpected narrowness in observed flow from a QPC⁵, but until now, high-resolution, detailed images of electron flow from a QPC have been difficult to obtain and no observations or predictions for this type of strong branching behaviour have been published. The average electron flow reflected by the tip back through the QPC falls off approximately as $1/r^2$ with distance r from the QPC.

In order to explore the experimentally observed current flow, we numerically calculated a set of conducting wavefunctions through a

QPC with disordered background potentials. Our model for the potential landscape incorporates known properties of 2DEGs in GaAs/AlGaAs heterostructures^{14,15} and replicates the physical parameters of the experimental system. To model the full in-plane potential, we consider two contributions. The first contribution is from the negatively charged gates that define the QPC, which we model using a smooth analytic potential that reproduces the quantized conductance steps characteristic of the QPC. The Fermi level remains constant inside the 2DEG, so that the propagation there is primarily affected by the second piece of the potential, the disordered background. There are two contributions to this background that we considered: the donor dopant atoms and unwanted impurities. For the impurities, distributed throughout the crystal structure, we take a random distribution in three dimensions and match the impurity atom density with a reasonable estimate for the physical sample ($1.25 \times 10^{15} \text{ cm}^{-3}$). The donors are located in a plane displaced from the 2DEG by 22 nm with a sheet density of $8 \times 10^{12} \text{ cm}^{-2}$; we estimate that half of the donors are ionized. Their distribution is random in space except for correlations limiting the maximum local density¹⁴. We use a $1/r^3$ potential at large distances for the impurities and donors, where r is the distance between a location in the plane of the 2DEG and the location of a given impurity or donor atom in the crystal. This $1/r^3$ dependence is the key feature of the full screened potential in a 2DEG from a point charge¹⁵.

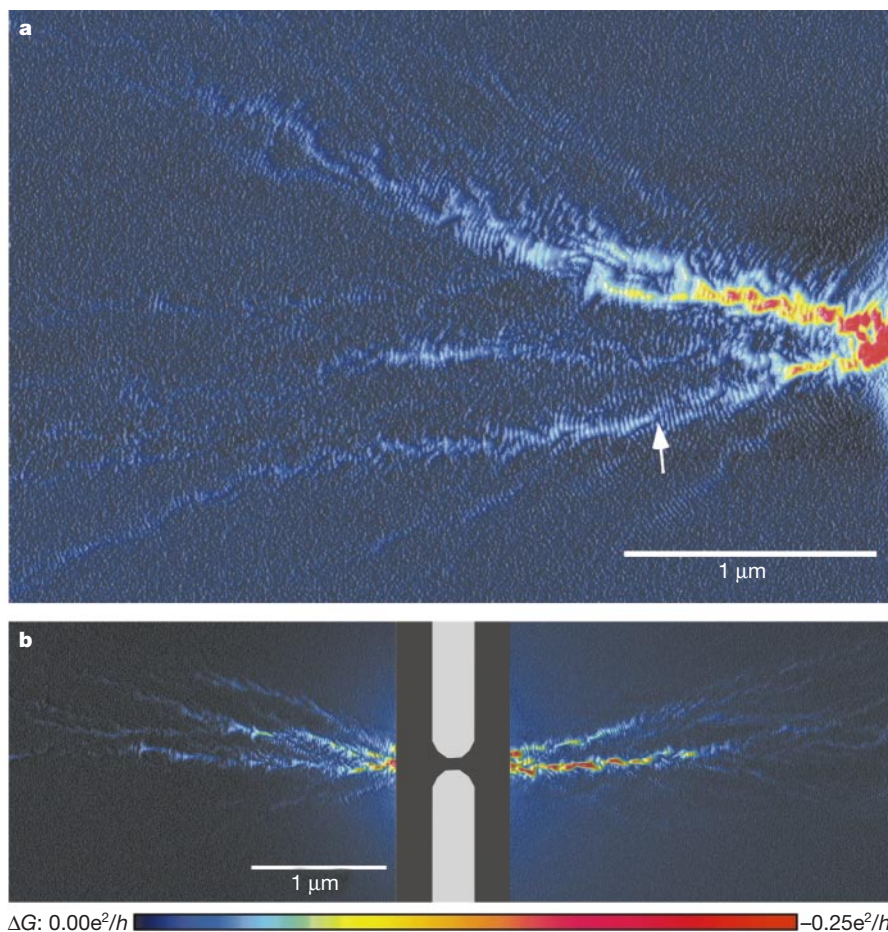


Figure 2 Experimental images of electron flow. **a**, Image of electron flow from one side of a QPC at $T = 1.7$ K, biased on the $G = 2e^2/h$ conductance step. Dark regions correspond to areas where the tip had little effect on QPC conductance, and hence are areas of low electron flow. The colour varies and the height in the scan increases with increasing electron flow. Narrow branching channels of electron flow are visible, and fringes spaced

by $\lambda_F/2$, half the Fermi wavelength, are seen to persist across the entire scan. **b**, Images of electron flow from both sides of a different QPC, again biased on the $G = 2e^2/h$ conductance step. The gated region in the centre was not scanned. Strong channelling and branching are again clearly visible. The white arrow points out one example of the formation of a cusp downstream from a dip in the potential.

Using the values for donor inhomogeneity and impurity density expected for the 2DEG sample in our model¹⁴, we calculated the mobility classically using the momentum relaxation time for an appropriate ensemble of trajectories and found it to match the measured value to within 10%. The distribution of energies in the disordered potential is very nearly gaussian with a standard deviation of about 8% E_F . The correlation length of the disordered potential is about 25 nm, that is, of the order of the wavelength.

In Fig. 3a we show a typical potential used in both classical and quantum simulations. Figure 3b and c shows the results of classical and quantum-mechanical flux density calculations in that potential which clearly show branched flow. The agreement between the classical and quantum results is very good, leading to the conclusion that the branched flow is essentially a classical phenomenon. Though there are occasional events where the flow is split by an impurity near the 2DEG, most of the bumps in the potential are well below the Fermi energy of the electrons. Locally, potential valleys act like lenses that focus the electron paths, albeit not perfectly, giving rise to a near-focal point known as a cusp. One example of such a cusp in the experimental images may be seen in Fig. 2a, as indicated by the arrow. The stronger branches surviving at large distances are the indirect result of passing over many hills and valleys (S.E.J.S. and E.J.H., manuscript in preparation), as shown in Fig. 3.

This classical phenomenon is robust, and it is seen in smooth potentials of disparate origin with features generally well below the energy of the scattered particles. The length scale for the formation of the channels is determined by the autocorrelation length of the potential. This regime of classical dynamics in a random potential

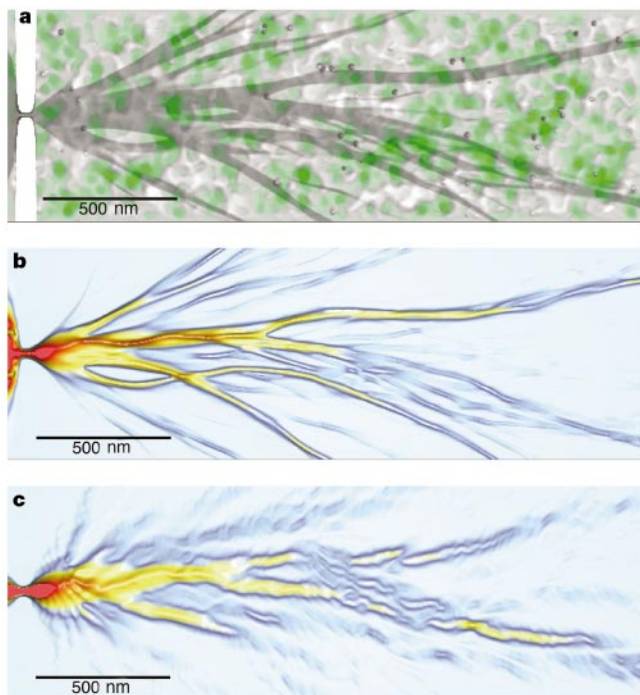


Figure 3 Calculated electron flow. **a**, Surface plot of the random potential for computed electron flow, including contributions from impurities, donors, and gates; green areas are low and white areas are high potential. The ‘shadow’ is cast by classical flux through the same potential. We note that the branched flux does not follow valleys in the potential. **b**, Classical and **c**, quantum-mechanical flux of electrons flowing through the potential in **a**. In the classical case, we followed the dynamics of an appropriate ensemble of classical trajectories and show the classical flux density. The quantum-mechanical results show the flux density of the transmitted wavefunction, coming through the point contact on the left. We note that both results show the same branching behaviour.

has not been studied in detail, falling as it does between the well explored extremes of gaussian white noise and widely spaced point scatterers. A detailed study of this phenomenon will appear elsewhere (S.E.J.S. and E.J.H., manuscript in preparation). Similar scattering, with the unexpected resulting strands of concentration of flux, might be expected in widely different contexts, such as sound propagation through the ocean, where it has recently been discussed¹⁶.

The experimental images in Fig. 2 show the position-dependent effect of the SPM tip on the conductance through the device. The charged tip induces an approximately lorentzian bump in the potential¹⁷ seen by electrons propagating through the system; we can simulate the experiments by adding a lorentzian to the potential at the tip position. Figure 4a shows the overall computed current flow through the device before the addition of a lorentzian. We compared the simulated flux in a small patch (Fig. 4b) with the conductance as a function of lorentzian position (Fig. 4c). This comparison confirms the relationship between flux and the images achieved by the experimental technique.

A striking feature of the experimental images (Fig. 2a and b) is the appearance of fringes oriented perpendicularly to electron flow and spaced by $\lambda_F/2$, half the Fermi wavelength. These fringes are caused by coherent constructive and destructive backscattering of electrons from the tip. In the region close to the point contact the fringes can be explained by multiple reflections of electron waves between the tip and the QPC gates. At farther distances two effects could suppress the fringes: phase decoherence and thermal broadening. In our sample the phase coherence length, $l_\phi = 18 \mu\text{m}$ ¹⁸, is much larger than our scan area and thus not a concern. The thermal length $l_{th} = \hbar 2\pi / m\lambda_F k_B T = 1.4 \mu\text{m}$ (where T is temperature, k_B is Boltzmann’s constant, \hbar is Planck’s constant divided by 2π , m is the mass of the electron, and λ_F is the Fermi wavelength), the distance over which electrons differing in energy by $k_B T$ drift 1 radian out of phase, is relevant. The fringes in our experimental and theoretical images, however, persist up to this length and beyond.

The persistence of the fringes can be explained by an unusual source of coherent backscattering (S.E.J.S., R.F. and E.J.H., manu-

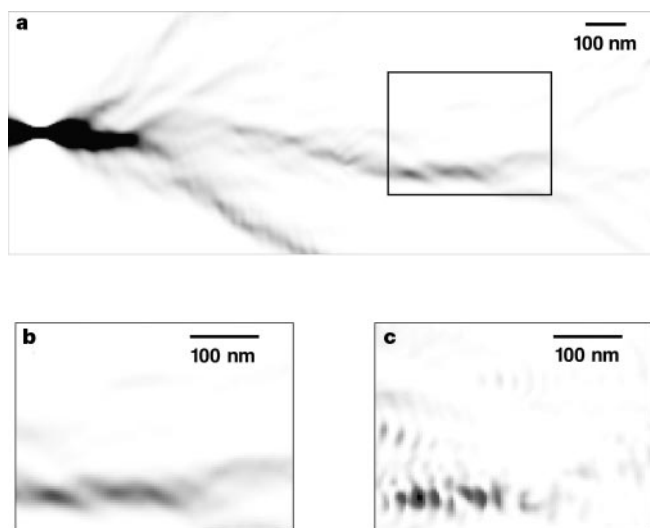


Figure 4 Calculated tip scan. **a**, Quantum-mechanical flux through a random potential. **b**, The flux from the boxed area in **a**. **c**, A raster scan of conductance as a function of SPM tip position in the same system as **a** and **b**. The conductance image in the model corresponds to the flux image, confirming our assertion that the experiment images electron flow. Additionally, the simulation **c** shows quantum fringes, as seen in the experiment. Though this simulation is at zero temperature, the fringes do survive thermal averaging.

script in preparation). The electron waves that are backscattered from the depletion region under the tip (located a distance r_{tip} from the QPC), interfere with a combination of the backscattered waves from all impurities in a ring covering the area $r_{\text{tip}} \pm l_{\text{th}}$ away from the QPC to produce alternating constructive and destructive total interference as r_{tip} is changed. As the tip is moved, the phase of the waves backscattered from the tip seen at the QPC varies as $2r_{\text{tip}}k$, where k is the wavevector. Importantly, this mechanism is resistant to thermal broadening, because as k is varied around k_F the phases of backscattered waves returning from impurities within the radius $r_{\text{tip}} \pm l_{\text{th}}$ vary in step with the phase from the tip (S.E.J.S., R.F. and E.J.H., manuscript in preparation) with the result that the fringes can easily survive. This mechanism requires phase-coherent transport over the round-trip distance to the most remote fringes, and may provide a new direct way to measure electron wave coherence length.

Another unusual feature of the fringes is that their separations are smaller than the width of the Lorentzian perturbation used in making the measurements. The tip perturbation has an estimated half-width at half-maximum of ~ 60 nm, based on electrostatic simulations (ref. 17 and M.A.T. *et al.*, manuscript in preparation). Our numerical work, however, gives evidence that the relevant feature is the presence of a classically forbidden “depletion region” beneath the tip. The edge of this depletion region provides the backscattering needed to direct electrons back through the QPC. This result is in accord with experimental findings that images of electron flow are only observed when the voltage on the tip is sufficient to create a small depletion region in the 2DEG (M.A.T. *et al.*, manuscript in preparation). Moreover, backscattering reflection from a circular depletion region where paths reverse and lead back to the QPC comes only from a small zone on the depletion region.

The information about electron flow made available by this imaging technique has several important implications and possible future applications. The observation that electrons can flow through a 2DEG in narrow, branching channels may be important for experiments relying on the assumption of ‘ballistic’ flow of electrons for distances less than the mean free path. Such detailed images of electron flow may also prove valuable in future explorations of spin transport for spintronics and possibly allow novel quantum computer implementations. The surprising persistence of coherent fringes well past the thermal length may help provide additional insight into a broad range of coherent phenomena including universal conductance fluctuations, phase coherence, and weak localization. This imaging technique can provide much detail about coherent electron flow, and is an important tool in investigating the underlying physics as well as the future design of 2DEG nanostructures. □

Received 25 October 2000; accepted 2 January 2001.

1. Beenakker, C. W. J. & van Houten, H. in *Solid State Physics* (eds Ehrenreich, H. & Turnbull, D.) 44, 1–228 (Academic, New York, 1991).
2. Sohn, L. L., Kouwenhoven, L. P. & Schon, G. *Mesoscopic Electron Transport in Semiconductor Nanostructures* (Kluwer Academic, Boston, 1997).
3. Topinka, M. A. *et al.* Imaging coherent electron flow from a quantum point contact. *Science* **289**, 2323–2326 (2000).
4. Eriksson, M. A. *et al.* Cryogenic scanning probe characterization of semiconductor nanostructures. *Appl. Phys. Lett.* **69**, 671–673 (1996).
5. Crook, R., Smith, C. G., Simmons, M. Y. & Ritchie, D. A. Imaging cyclotron orbits and scattering sites in a high-mobility two-dimensional electron gas. *Phys. Rev. B* **62**, 5174–5178 (2000).
6. Crook, R. *et al.* Imaging diffraction-limited electronic collimation from a non-equilibrium one-dimensional ballistic constriction. *J. Phys. Cond. Matter* **12**, L167–L172 (2000).
7. McCormick, K. L. *et al.* Scanned potential microscopy of edge and bulk currents in the quantum Hall regime. *Phys. Rev. B* **59**, 4654–4657 (1999).
8. Zhitenev, N. B. *et al.* Imaging of localized electronic states in the quantum Hall regime. *Nature* **404**, 473–476 (2000).
9. Finkelstein, G., Glicofridis, P. I., Ashoori, R. C. & Shayegan, M. Topographic mapping of the quantum Hall liquid using a few-electron bubble. *Science* **289**, 90–94 (2000).
10. Manoharan, H. C., Lutz, C. P. & Eigler, D. M. Quantum mirages formed by coherent projection of electronic structure. *Nature* **403**, 512–515 (2000).
11. Jamneala, T., Madhavan, V., Chen, W. & Crommie, M. F. Scanning tunneling spectroscopy of transition-metal impurities at the surface of gold. *Phys. Rev. B* **61**, 9990–9993 (2000).

12. Yoo, M. J. *et al.* Scanning single-electron transistor microscopy: imaging individual charges. *Science* **276**, 579–582 (1997).
13. Gurevich, L., Canali, L. & Kouwenhoven, L. P. Scanning gate spectroscopy on nanoclusters. *Appl. Phys. Lett.* **76**, 384–386 (2000).
14. Grill, R. & Döhler, G. H. Effect of charged donor correlation and Wigner liquid formation on the transport properties of a two-dimensional electron gas in modulation delta-doped heterojunctions. *Phys. Rev. B* **59**, 10769–10777 (1999).
15. Davies, J. H. *The Physics of Low-Dimensional Semiconductors: An Introduction* (Cambridge Univ. Press, New York, 1998).
16. Wolfson, M. A. & Tomsovic, S. On the stability of long-range sound propagation through a structured ocean. At (xxx.lanl.gov/abs/nlin.CD/0002030) (2000).
17. Eriksson, M. A. *et al.* Effect of a charged scanned probe microscope tip on a subsurface electron gas. *Superlattices Microstruct.* **20**, 435–440 (1996).
18. Althuler, B. L., Aronov, A. G. & Khmel'nitsky, D. E. Effects of electron-electron collisions with small energy transfers on quantum localisation. *J. Phys. C* **15**, 7367–7386 (1982).

Acknowledgements

This work was supported in part at Harvard University by the Office of Naval Research/Augmentation Awards for Science and Engineering Research Training (ONR/AASERT), by ONR and by the National Science Foundation through grants for the Materials Research Science and Engineering Center and for the Institute for Theoretical Atomic and Molecular Physics at Harvard University and Smithsonian Astrophysical Observatory. Work at the University of California Santa Barbara was supported by the NSF Science and Technology Center QUEST.

Correspondence and requests for materials should be addressed to R.M.W. (e-mail: westervelt@deas.harvard.edu).

Strongly linked current flow in polycrystalline forms of the superconductor MgB₂

D. C. Larbaestier*[†], L. D. Cooley*, M. O. Rikel*, A. A. Polyanskii*, J. Jiang*, S. Patnaik*, X. Y. Cai*, D. M. Feldmann*, A. Gurevich*, A. A. Squitieri*, M. T. Naus*, C. B. Eom*[†], E. E. Hellstrom*[‡], R. J. Cava[‡], K. A. Regan[‡], N. Rogado[‡], M. A. Hayward[‡], T. He[‡], J. S. Slusky[‡], P. Khalifah[‡], K. Inumaru[‡] & M. Haas[‡]

* Applied Superconductivity Center, University of Wisconsin–Madison, 1500 Engineering Drive, Madison, Wisconsin 53706, USA

† Department of Materials Science and Engineering, University of Wisconsin–Madison, 1509 University Avenue, Madison, Wisconsin 53706, USA

‡ Department of Chemistry and Princeton Materials Institute, Princeton University, Princeton, New Jersey 08544, USA

The discovery of superconductivity at 39 K in magnesium diboride¹, MgB₂, raises many issues, a critical one being whether this material resembles a high-temperature copper oxide superconductor or a low-temperature metallic superconductor in terms of its behaviour in strong magnetic fields. Although the copper oxides exhibit very high transition temperatures, their in-field performance² is compromised by their large anisotropy, the result of which is to restrict high bulk current densities to a region much less than the full magnetic-field–temperature (H – T) space over which superconductivity is found. Moreover, the weak coupling across grain boundaries makes transport current densities in untextured polycrystalline samples low and strongly sensitive to magnetic field^{3,4}. Here we report that, despite the multiphase, untextured, microscale, subdivided nature of our MgB₂ samples, supercurrents flow throughout the material without exhibiting strong sensitivity to weak magnetic fields⁵. Our combined magnetization, magneto-optical, microscopy and X-ray investigations show that the supercurrent density is mostly determined by flux pinning, rather than by the grain boundary connectivity. Our results therefore suggest that this new superconductor class is not